DISCOVERY POTENTIAL FOR SM HIGGS WITH $H \to ZZ^{(*)} \to 4l$ AT CMS*

Paolo Meridiani

On behalf of the CMS Collaboration

INFN Roma1, Piazzale Aldo Moro 2, 00185 Roma, Italy

(Received November 15, 2006)

A prospective analysis is presented for the discovery potential and properties measurement of the Standard Model Higgs boson with the CMS experiment at the LHC collider. The analysis focuses on the $H \to ZZ^{(*)} \to 4l{+}X$ channel for Higgs boson masses in the range $120 \lesssim m_H \lesssim 600$ GeV/c^2. It relies on a full simulation of the detector response and usage of detailed lepton reconstruction tools. Emphasis is put on realistic strategies for the evaluation of experimental systematics and control of physics background processes.

PACS numbers: 14.80.Bn

1. Introduction

The cleanest and golden road towards a discovery at the LHC of the Standard Model Higgs boson is via single Higgs production followed by a cascade decay into charged leptons, $H \to ZZ^{(*)} \to l^+l^-l^+l^-$. Depending on the flavour of the leptons from the Z decay, three different topologies can be identified: $H \to 4e$, $H \to 4\mu$, $H \to 2e2\mu$.

One of the good features of this channel, apart for its clean signature with relatively small background, is that it can provide a precision determination of the Higgs boson mass, width and production cross-section.

The discovery potential of the CMS experiment for the SM Higgs boson in this channel has been evaluated in the mass range of $120 \leq m_H \leq 600$ GeV/c^2 . The analysis presented in this paper relies on a detailed simulation of the detector response in the experimental conditions of the first years of low luminosity LHC running. Details on the signal and background Monte Carlo samples are given in Section 2.

* Presented at the "Physics at LHC" Conference, Kraków, Poland, July 3–8, 2006.

Simple observables from the lepton reconstruction coupled with basic event kinematics are used to select the signal and reduce the background, as it is described in Section 3. The selections are optimised to have the highest significance for a discovery. Overall, the emphasis is put on realistic strategies for the control of experimental errors and the estimation of systematic uncertainties on the physics background rates. These are described in Section 4.

All the analyses described here are present in the volume II of the CMS Physics TDR [2] where the reader is directed for further details. Details of each single channel, $4e$ 4μ $2e2\mu$, can also be found in several CMS notes: [3–6].

2. Signal and background samples

Both signal and background event samples are generated at the Leading Order (LO) approximation, and Next to Leading Order (NLO) production cross-sections are used for their normalisation.

The Higgs boson signal is simulated with PYTHIA [7]; either gluon fusion or weak boson fusion have been activated. Values of the total cross-section at NLO are calculated including all Higgs production processes via HIGLU [8], the branching ratio BR($H \to ZZ^{(*)}$) is computed via HDECAY [9].

In the $4e$ and 4μ channel channels an enhancement of the signal is due to the constructive final state interference between like-sign electrons originating from different $Z^{(*)}$ bosons [10]. This enhancement has been re-evaluated with COMPHEP [11] and amounts to a factor 1.130 ± 0.006 at $m_H = 115\text{GeV}/c^2$, slowly decreasing to a negligible value when approaching $m_H \approx 2m_Z$.

The background taken into account consists of three samples: the irreducible background represented by the $ZZ^{(*)}$ SM background continuum and the reducible background composed of $t\bar{t}$ and $Zb\bar{b}$.

The $ZZ^{(*)}$ SM background continuum is generated using either PYTHIA or COMPHEP. PYTHIA includes only the t-channel contribution in the $q\bar{q}$ initial state, while the s-channel, included in COMPHEP, might contribute up to 10% for low Higgs boson masses and can be neglected for higher masses. To account for contributions due to all the NLO diagrams and to the NNLO gluon fusion ($gg \to ZZ$ contributes $\sim 20\%$ with respect to the LO [10] cross section), events are reweighted with a m_{4l} dependent K-factor $K(m_{4l}) = K_{\text{NLO}}(m_{4l}) + 0.2$. The total NLO cross-section is estimated to be 29 pb for this process.

The $t\bar{t}$ background sample is also generated with PYTHIA, with W bosons and τ leptons forced to leptonic decays, but with b quarks left to decay freely. Both gluon fusion and quark annihilation initial states are simulated and the cross-section normalised to the NLO value is 840 pb.

The $Zb\bar{b}$ background is generated using all lowest order $gg \to l^+l^-b\bar{b}$ and $qq' \to l^+l^-b\bar{b}$ diagrams calculated with COMPHEP and interfaced with PYTHIA for showering and hadronisation. A NLO K-factor of 2.4 ± 0.3 is estimated, yielding a final cross-section for this channel of 276 pb.

3. Event reconstruction and selection

An efficient and precise lepton reconstruction plays a fundamental role in this channel, which can be considered as a benchmark for the lepton reconstruction.

Details on the lepton reconstruction algorithms and their characteristics can be found in the volume I of the CMS Physics TDR [1], while here only the features relevant to the analysis will be outlined.

3.1. Electron reconstruction

Elaborate electron reconstruction procedures have been introduced very recently in CMS [13]. The electron identification and momentum measurements, especially for electrons with p_{T} below 50 GeV/c, are somewhat distorted by the amount of tracker material which is distributed in front of the ECAL, and by the presence of a strong magnetic field aligned with the collider beam z axis.

The procedures introduced in Ref. [13] provide new useful observables that allow to better deal with these detector effects, combining information from the pixel detector, the silicon strip tracker and the electromagnetic calorimeter. The energy deposited in the electromagnetic calorimeter is measured in clusters of clusters (superclusters) which partially recover bremsstrahlung photons emitted along the electron trajectory in the tracker volume. The electron tracks are built from seeds in the pixel detector found via a cluster-driven pixel hit matching algorithm, followed by a reconstruction of trajectories in the silicon strip tracker with a Gaussian Sum Filter algorithm, using a specific energy loss modelling [14].

Electrons are classified using observables sensitive to the pattern of bremsstrahlung emission, involving recognition of distinct track-supercluster patterns. This gives the ability to distinguish between electrons emitting a small or a large fraction of their energy in bremsstrahlung. The initial electron energy can be then deduced from a weighted combination of the supercluster energy and tracker momentum measurements.

Basic pre-selection requirements are assigned to the electrons, in order to reduce possible background sources involving "fake" electrons contamination from QCD jets. A threshold on the p_{T} at the level of $p_{\mathrm{T}} > 5$ GeV/c is also applied.

3.2. Muon reconstruction

Muon reconstruction is performed in 3 stages: local reconstruction (local-pattern recognition), stand alone reconstruction and global reconstruction. Starting from a seed, the chambers compatible with the seed are identified and local reconstruction is performed only in the muon detector. The global-muon reconstruction uses also silicon tracker hits, and the combination of the tracker measurement improves the momentum estimation of a factor around 10.

In order to minimise muon reconstruction systematic uncertainties, only those reconstructed muons that have transverse momentum $p_{\mathrm{T}} > 7$ GeV/c are selected in the barrel, and those with momentum $p > 13$ GeV/c in the endcaps. Below these thresholds a quick drop of the efficiency is observed. These cuts do not affect the number of accepted signal events significantly.

3.3. Event selection

The $H \rightarrow 4l$ signal presents a characteristic topology, which consists of almost two opposite charged lepton-pairs in the final state. All leptons are isolated and their invariant mass should be around the Z-boson mass, depending on the restrictions in the phase space introduced by the Higgs boson mass itself. The four-lepton invariant mass peaks around the Higgs boson mass.

In $Zb\bar{b}$ and $t\bar{t}$ background events, two of the leptons come from b-quark decays and are usually found within a jet (*i.e.*, non-isolated), have lower transverse momenta and often exhibit detectable displaced vertices.

The most discriminative criteria is the isolation, defined as the amount of transverse energy in the calorimeter (calorimeter isolation), or the sum of the transverse momentum of the tracks reconstructed in the tracker (tracker isolation), inside a cone in η–ϕ space around each lepton. Typical rejection obtained from isolation is between 20 for $Zb\bar{b}$ and 100 for $t\bar{t}$ given an efficiency of 90% on the signal.

In addition to isolation, a vertex constraint can be imposed on the transverse impact parameter of the leptons to further suppress $Zb\bar{b}$ and $t\bar{t}$. A rejection factor from 2 to 5 on these background can be achieved for 90–95% signal efficiency.

Different strategies for kinematical cuts can be adopted: in particular cuts can be applied on the p_{T} of each lepton, giving a reduction greater

than 4 on $Zb\bar{b}$ and $t\bar{t}$. Also cuts can be put on one lepton pair mass, which is required to be around the Z nominal mass; this allows a further reduction of a factor 2 on the $t\bar{t}$ background.

The final selection efficiency, defined with respect to the trigger accepted events (CMS Level1 and High Level Trigger are highly efficient, >95%, on this channel) is shown in Fig. 1(a) as a function of the Higgs mass; as an example the $2e2\mu$ channel is considered. Selection efficiency significantly varies for different Higgs mass hypotheses, ranging between 25% and 55%.

A plot of the 4-lepton invariant mass after all selections is shown in Fig. 1(b) for the Higgs mass hypothesis of $m_H = 140\text{GeV}/c^2$; it can be seen that the $Zb\bar{b}$ and $t\bar{t}$ are almost fully suppressed, while the only remaining background is the $ZZ^{(*)}$ continuum.

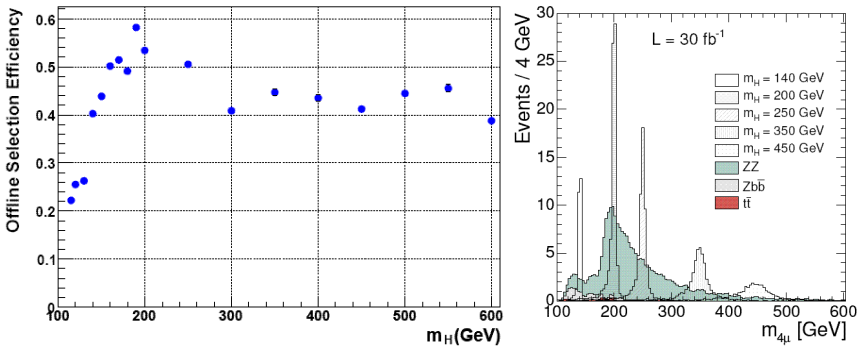

(a) (b)

Fig. 1. (a) Final selection efficiency, defined with respect to the trigger accepted events; as an example the $2e2\mu$ channel is considered (b) Lepton invariant mass after all selections for signal and background; various Higgs mass hypotheses have been used.

4. Systematics

The main systematic effect considered in the analysis is represented by the evaluation of mean background events in the signal region; since after the application of the selection criteria only the $ZZ^{(*)}$ continuum remains as the dominant or sole background over the full mass range the study has been reduced to this channel.

Both theoretical and experimental systematics have been considered; the strategy used has been to evaluate the background directly from the data. A reduction of the PDF and QCD scale uncertainty, and a complete cancellation of the luminosity uncertainty, is achieved either normalising to the $Z \to 2l$ data or to sidebands. Theoretical uncertainty goes from 2 to 8% for

normalisation to $Z \to 2l$, and from 0.5 to 4% for the normalisation to sidebands. The sidebands method, however, is limited by statistical uncertainty, due to low number of selected $ZZ^{(*)}$ events.

The main experimental systematics which have been considered are on the lepton reconstruction and selection (isolation) efficiencies and on the energy and momentum scales. It is possible to control the lepton reconstruction at the required precision using leptons from the W and Z decays. In fact, the huge cross-sections of these two processes will allow for a significant reduction of reconstruction uncertainties already after few fb^{-1}. Other experimental effects which have been taken into account are the trigger efficiencies and the knowledge of the material budget. With 1–2 fb^{-1} experimental systematics are estimated to be below 1%.

5. Discovery reach

Fig. 2 shows the luminosity needed for a 5σ discovery for the $H \to 4l$ channel compared with $H \to \gamma\gamma$ and $H \to 2l2\nu$ as a function of m_H; on the right the expected significance of the $H \to 4l$ signal observation for an integrated luminosity of 30 fb^{-1} is shown as a function of the Higgs mass and is compared to other channels reach. Systematic errors have been included in these plots. It can be argued that less than 10 fb^{-1} are required for a 5σ discovery in the channel $H \to 4l$ in the mass range $130 < m_H < 160\text{GeV}/c^2$ and $2m_Z < m_H < 550$ GeV/c^2. The discovery in the Higgs mass range not covered by the $H \to 4l$ channel, between 160 GeV/c^2 and $2m_Z$, is possible using the complementary channel $H \to WW^{(*)} \to 2l2\nu$. For masses below 130 GeV/c^2 the highest discovery potential is obtained in the $H \to 2\gamma$ channel.

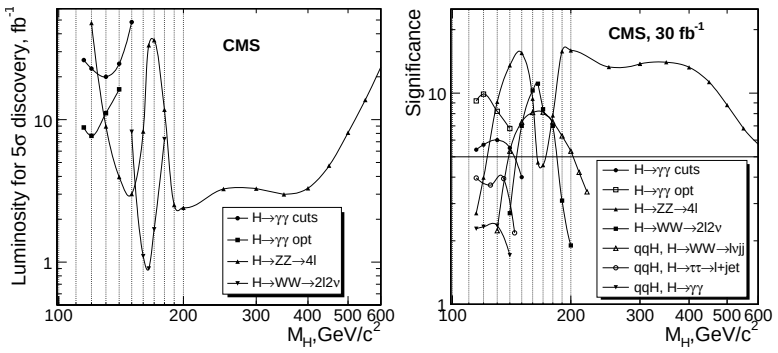

(a) (b)

Fig. 2. (a) Luminosity needed for a 5σ discovery for the $H \to 4l$ channel compared with $H \to \gamma\gamma$ and $H \to 2l2\nu$ as a function of m_H. (b) Expected significance of the $H \to 4l$ signal observation for an integrated luminosity of 30 fb^{-1}.

5.1. Mass measurement

Fig. 3(a) shows the statistical precision of the determination of the Higgs boson mass for an integrated luminosity of 30 fb^{-1} as a function of the mass hypothesis; for comparison purposes values from the $H \to \gamma\gamma$ channel are reported as well. Over the entire mass range considered a precision in the mass determination of better than 1% can be attained.

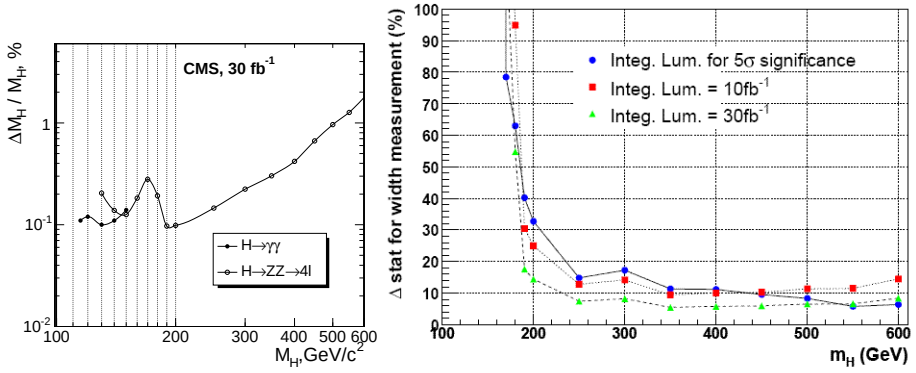

(a) (b)

Fig. 3. Statistical error on the determination of the Higgs boson (a) mass and (b) width as a function of the mass hypothesis for an integrated luminosity of 30 fb^{-1} (for the width also 10 fb^{-1} and the luminosity corresponding to a 5σ significance are reported). On the (a) plot for comparison the precision in the $H \to \gamma\gamma$ channel is reported as well.

5.2. Width measurement

The width measurement is possible only for values of m_H above 200 Gev/c^2, when the Higgs natural width starts to dominate the experimental resolution. Fig. 3(b) shows the statistical error on the determination of natural width of the Higgs boson, obtained from a fit to the invariant mass distribution. The direct measurement of the Higgs boson width is achievable with a precision of better than 30% for $m_H \geq 200$ GeV/c^2.

6. Summary

A prospective analysis has been performed for the search of the Standard Model Higgs boson decaying in a $ZZ^{(*)}$ pair and subsequently to leptons in the context of the CMS detector; the analysis includes an evaluation of the main systematic effects.

It has been shown that less than 10 fb^{-1} are required for a 5σ discovery in this channel for Higgs masses lying in the range $130 < m_H < 160$ GeV/c^2

and $2m_Z < m_H < 550$ GeV/c^2. The channel allows the measurement of the properties of the Higgs boson; in particular the mass can be precisely measured within 1% and the width can be measured to better than 30% for $m_H \geq$200 GeV/c^2.

REFERENCES

[1] CMS Collaboration, Physics TDR Vol. I, CERN/LHCC 2006-001.

[2] CMS Collaboration, Physics TDR Vol. II, CERN/LHCC 2006-021.

[3] S. Abdullin *et al.*, Search Strategy for the Standard Model Higgs Boson in the $H \to ZZ^{(*)} \to 4\mu$ Decay Channel Using $m(4mu)$ Dependent Cuts, CMS NOTE-2006/122.

[4] M. Aldaya *et al.*, Discovery Potential and Search Strategy for the Standard Model Higgs Boson in the $H \to ZZ^{(*)} \to 4\mu$ Decay Channel Using a Mass-Independent Analysis, CMS NOTE-2006/106.

[5] S. Baffioni *et al.*, Discovery Potential for the SM Higgs Boson in the $H \to ZZ^{(*)} \to 4e$ Decay Channel, CMS NOTE-2006/115.

[6] D. Futyan *et al.*, Search for the Standard Model Higgs Boson in the Two-Electron and Two-Muon Final State with CMS, CMS NOTE-2006/136.

[7] T. Sjostrand, L. Lonnblad, S. Mrenna, `hep-ph/0108264`.

[8] M. Spira, *Nucl. Instrum. Methods Phys. Res.* **A389**, 357 (1997); M. Spira, `hep-ph/9510347`.

[9] A. Djouadi, J. Kalinowski, M. Spira, *Comput. Phys. Commun.* **108**, 56 (1998).

[10] C. Zecher, T. Matsuura, J.J. van der Bij, *Z. Phys.* **C64**, 219 (1994).

[11] E. Boos *et al.* (CompHEP Collaboration), *Nucl. Instrum. Methods Phys. Res.* **A534**, 250 (2004); A. Pukhov *et al.*, CompHEP — a Package for Evaluation of Feynman Diagrams and Integration over Multi-Particle Phase Space, Moscow State U. preprint INP-MSU-98-41-542.

[12] J.M. Campbell, R.K. Ellis, MCFM — Monte Carlo for FeMtobarn processes, `http://mcfm.fnal.gov`.

[13] S. Baffioni *et al.*, Electron Reconstruction in CMS, CMS NOTE-2006/040.

[14] W. Adam, R. Frühwirth, A. Strandlie, T. Todorov, Reconstruction of Electrons with the Gaussian-Sum Filter in the CMS Tracker at the LHC, CMS NOTE-2005/001.